

Magnetic excitations and phonons simultaneously studied by resonant inelastic x-ray scattering in optimally doped $\text{Bi}_{1.5}\text{Pb}_{0.55}\text{Sr}_{1.6}\text{La}_{0.4}\text{CuO}_{6+\delta}$

Y. Y. Peng,^{1,*} M. Hashimoto,² M. Moretti Sala,³ A. Amorese,^{1,†} N. B. Brookes,³
 G. Dellea,¹ W.-S. Lee,⁴ M. Minola,^{1,‡} T. Schmitt,⁵ Y. Yoshida,⁶ K.-J. Zhou,^{5,§}
 H. Eisaki,⁶ T. P. Devereaux,⁴ Z.-X. Shen,^{4,7} L. Braicovich,^{1,8} and G. Ghiringhelli^{1,8}

¹*Dipartimento di Fisica, Politecnico di Milano, Piazza Leonardo da Vinci 32, I-20133 Milano, Italy*

²*Stanford Synchrotron Radiation Lightsource, SLAC National Accelerator Laboratory, 2575, Sand Hill Road, Menlo Park, California 94025, USA*

³*European Synchrotron Radiation Facility (ESRF), BP 220, F-38043 Grenoble Cedex, France*

⁴*Stanford Institute for Materials and Energy Sciences, SLAC National Accelerator Laboratory, 2575 Sand Hill Road, Menlo Park, CA 94025, USA*

⁵*Swiss Light Source, Paul Scherrer Institut, CH-5232 Villigen PSI, Switzerland*

⁶*Nanoelectronics Research Institute, AIST, Ibaraki 305-8568, Japan*

⁷*Geballe Laboratory for Advanced Materials, Departments of Physics and Applied Physics, Stanford University, CA 94305, USA*

⁸*CNR-SPIN, CNISM, Politecnico di Milano, Piazza Leonardo da Vinci 32, I-20133 Milano, Italy*
 (Dated: September 25, 2021)

Magnetic excitations in the optimally doped high- T_c superconductor $\text{Bi}_{1.5}\text{Pb}_{0.55}\text{Sr}_{1.6}\text{La}_{0.4}\text{CuO}_{6+\delta}$ (OP-Bi2201, $T_c \simeq 34$ K) are investigated by Cu L_3 edge resonant inelastic x-ray scattering (RIXS), below and above the pseudogap opening temperature. At both temperatures the broad spectral distribution disperses along the (1,0) direction up to ~ 350 meV at zone boundary, similarly to other hole-doped cuprates. However, above ~ 0.22 reciprocal lattice units, we observe a concurrent intensity decrease for magnetic excitations and quasi-elastic signals with weak temperature dependence. This anomaly seems to indicate a coupling between magnetic, lattice and charge modes in this compound. We also compare the magnetic excitation spectra near the anti-nodal zone boundary in the single layer OP-Bi2201 and in the bi-layer optimally doped $\text{Bi}_{1.5}\text{Pb}_{0.6}\text{Sr}_{1.54}\text{CaCu}_2\text{O}_{8+\delta}$ (OP-Bi2212, $T_c \simeq 96$ K). The strong similarities in the paramagnon dispersion and in their energy at zone boundary indicate that the strength of the super-exchange interaction and the short-range magnetic correlation cannot be directly related to T_c , not even within the same family of cuprates.

PACS numbers: 74.72.Gh, 75.30.Ds, 74.25.Kc, 78.70.Ck

I. INTRODUCTION

In recent years, resonant inelastic x-ray scattering (RIXS) at the Cu L_3 edge, thanks to the strong spin-orbit coupling of the $2p_{3/2}$ core-hole intermediate state that provides a direct access to spin flip excitations,^{1,2} has become a powerful complement to neutron inelastic scattering for the determination of magnetic excitation dispersion in cuprates. The persistence of magnetic excitations has been observed from undoped antiferromagnetic insulators to overdoped superconductors, both for hole- and electron-doped compounds, across the respective superconducting domes.^{3–8} This confirms that short-range antiferromagnetic spin correlations survive to high doping and are exceptionally robust. These observations might imply that high energy magnetic fluctuations are necessary for superconductivity, although their possible role as pairing mechanism has not been demonstrated.

Moreover Cu L_3 resonant soft x-ray scattering has decisively contributed to reveal an electronic order now considered ubiquitous in the cuprate superconductors. Earlier evidence of bulk charge order was observed in La-based cuprates by neutron^{9,10} and x-ray scattering.¹¹ More recently, charge order along the Cu-O bond direction has been observed in (Y,Nd) $\text{Ba}_2\text{Cu}_3\text{O}_{6+x}$ (YBCO, NBCO),^{12–16} Bi-based cuprates $\text{Bi}_2\text{Sr}_{2-x}\text{La}_x\text{CuO}_{6+\delta}$

(Bi2201) and $\text{Bi}_2\text{Sr}_2\text{CaCu}_2\text{O}_{8+\delta}$ (Bi2212).^{17–19} The direct observation of charge order in cuprates came first in the underdoped regime, soon after for the optimal doping of hole-doped cuprates^{19,20} and very recently also in the electron-doped compounds.²¹ The temperature dependence of charge order in YBCO and Bi2212 displays its competition with superconductivity.^{13,15,18}

To comprehend the superconductivity of cuprates we need to take into account the diversity of electronic and magnetic excitations. Whether and how these excitations, such as charge, spin, lattice and orbital orders, interact with each other is still the matter of active research. One of the superiority of RIXS is that it can measure different kinds of excitations simultaneously. This allows us to discuss the interplay between the charge, spin, lattice and orbital orders more in detail within a single experiment. Further, temperature dependence may provide insights into their physical properties and about their role in superconductivity and pseudogap.

In this Article we study the collective excitations in the optimally doped $\text{Bi}_{1.5}\text{Pb}_{0.55}\text{Sr}_{1.6}\text{La}_{0.4}\text{CuO}_{6+\delta}$ (OP-Bi2201, $T_c \simeq 34$ K) by momentum resolved resonant inelastic x-ray scattering (RIXS) at the Cu L_3 edge. Considering that the recent angle-resolved photoemission spectroscopy (ARPES) study on OP-Bi2201 showed a particle-hole symmetry breaking and a phase tran-

sition below the pseudogap temperature $T^* \simeq 125$ K),^{22,23} our measurements were performed at two temperatures, 50 K (below T^*) and 200 K (above T^*). We also compare these results to those of optimally doped $\text{Bi}_{1.5}\text{Pb}_{0.6}\text{Sr}_{1.54}\text{CaCu}_2\text{O}_{8+\delta}$ (OP-Bi2212, $T_c \simeq 96$ K) to investigate the material dependence of magnetic excitation within the Bi-based superconductor family.

II. EXPERIMENTAL METHOD

The high quality OP-Bi2201 and OP-Bi2212 single crystals were grown by the floating zone method. The hole concentration was optimized by annealing the samples in N_2 flow. The RIXS experiments for OP-Bi2201 collected at 50 K and 200 K were performed with the SAXES instrument²⁴ at the ADDRESS beamline of the Swiss Light Source at the Paul Scherrer Institut,²⁵ the experimental energy resolution was ~ 150 meV; RIXS measurements for OP-Bi2201 and OP-Bi2212 collected at 40 K were performed with the AXES spectrometer at the beamline ID08 of the European Synchrotron Radiation Facility (ESRF),²⁶ the combined energy resolution was ~ 300 meV. The x-ray energy was tuned to the maximum of the Cu L_3 absorption peak around 931.3 eV. The elastic scattering position was determined with high accuracy for every momentum transfer by comparing the RIXS spectrum to that of polycrystalline graphite attached on the sample surface. Samples were cleaved in air some minutes before installation inside the ultrahigh vacuum measurement chamber ($\sim 3 \times 10^{-9}$ mbar).

The experimental geometry is shown in Fig. 1(a). X-rays are incident on the sample surface at θ_i and scattered by $2\theta = 130$ deg (constant). The scattering vector \mathbf{Q} is denoted using the pseudotetragonal unit cell with $a = b = 3.8$ Å and $c = 24.4$ Å for OP-Bi2201, with $a = b = 3.86$ Å and $c = 31$ Å for OP-Bi2212, where the axis c is normal to the cleaved sample surface. δ is the angle between total momentum \mathbf{Q} and sample c -axis. In the experiment δ is changed by rotating the sample around the vertical axis b in order to change Q_{\parallel} , the projection of the momentum transfer \mathbf{Q} along $[100]$. Here large negative Q_{\parallel} corresponds to near grazing-incidence geometry; large positive Q_{\parallel} corresponds to near grazing-emission geometry. The x-ray polarization can be chosen parallel (π) or perpendicular (σ) to the horizontal scattering plane. Fig. 1(b) shows the reciprocal space near the Brillouin zone center. The typical size of the Brillouin zone in cuprates is 0.81 Å⁻¹ (0.5 reciprocal lattice units, rlu) and the maximum of Q_{\parallel} for 930 eV photons is 0.77 Å⁻¹ (0.48 rlu) for $2\theta = 130$ deg. We measured along $(\pm 0.5, 0)$ direction and the thick green line represents the region explored in this work. We follow previous conventions²⁷ and present normalized spectra so that the integrated intensity of the dd excitations ($[-3, -1]$ eV) equals to one.

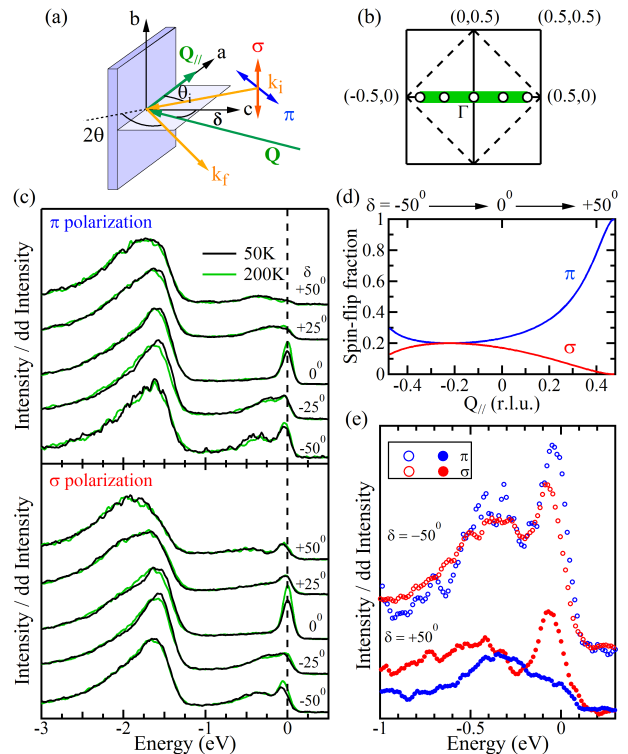


FIG. 1. (color online) (a) The experimental geometry. (b) Reciprocal-space image, the nuclear and magnetic first Brillouin zones are drawn with solid and dashed lines, respectively; the thick green line indicates the range covered by the experiments. (c) Representative RIXS spectra of OP-Bi2201 for various δ values in steps of 25 deg as indicated by the black empty circles in panel b, i.e. from 15 deg grazing incidence to 15 deg grazing emission, as measured with respect to the sample surface. Top: π polarized incident x-rays. Bottom: σ polarized incident x-rays. Data were collected at 50 K and 200 K. (d) Single spin-flip fraction (without orbital excitation) for π or σ polarizations according to RIXS cross section calculations for $2\theta = 130$ deg. The non-spin-flip channel can be spread over elastic, charge excitations, double-spin-flip excitations and phonons, covering a broad spectral range from 0 to 1 eV energy loss. This explains why spin-flip channel, less intense but more concentrated in energy, often the most easily recognizable spectral feature. (e) RIXS spectra measured at $Q_{\parallel} = -0.4$ rlu with grazing-incidence geometry ($\delta = -50$ deg) and measured at $Q_{\parallel} = 0.4$ rlu with grazing-emission geometry ($\delta = +50$ deg) for π - or σ -polarized light. Data were collected at 50 K. All spectra are normalized to the integrated intensity of the dd excitations.

III. RESULTS

Fig. 1(c) displays some RIXS spectra at representative δ angles for OP-Bi2201, collected at 50 K and 200 K with both π and σ polarized incident x-rays. The spectra exhibit, below -1.5 eV, dd excitations (transitions of the unpaired hole of Cu^{2+} from the $d_{x^2-y^2}$ to other d orbitals),²⁸⁻³⁰ with no obvious temperature dependence. Two broad peaks around -1.6 eV and around -1.9 eV

can be roughly ascribed to the transitions to the d_{xy} and $d_{xz/yz}$ orbitals, in analogy to the results obtained in the undoped compounds by Moretti Sala et al.²⁸ The $d_{3z^2-r^2}$ final state, more difficult to discern, is probably at slightly higher energy loss. The elastic peak is, as usual, stronger at specular angle ($\delta = 0$ deg) due to the reflectivity from the surface. The dispersion of the dd excitations is as small as that observed previously in other layered cuprates²⁸ within the energy resolution of our experiment.

In layered cuprates the simplest magnetic excitation implies the reversal of the spin 1/2 at one site, giving origin to a magnon in the antiferromagnetic parent compounds and to a so-called paramagnon in doped materials. In all cases the single spin-flip excitation is obtained through the rotation by 90 deg of the scattering photon polarization vector: it turns out that the only $\sigma\pi'$ and $\pi\sigma'$ combinations lead to non-zero spin-flip cross section, where the prime denotes the polarization of the scattered photon,^{1,31} because due to the x^2-y^2 symmetry of the $3d$ hole, the relevant polarization rotation is that projected on the ab plane. In Fig. 1(d) we show the spin-flip fraction as calculated with the simplified RIXS cross sections of Refs. 1, 27, and 28 for $2\theta = 130$ deg. The blue (red) line represents the spin-flip fraction of the low energy excitation spectral weight for incident π (σ) polarization. It must be kept in mind that, whereas the non-spin-flip part is spread over several contributions differing in nature (charge excitations, phonons, diffuse elastic, double spin-flip) and energy, the single spin-flip channel is concentrated in the resolution limited peak in the antiferromagnetic parent compounds or in the (often broad) paramagnon in the doped superconductors. This fact makes the spin-flip excitations more evident and recognizable with respect to the non-spin-flip excitations. We notice that, at grazing incidence (large negative δ values), the single spin-flip fraction is relatively small for both incident polarizations. This is particularly evident at $\delta = -50$ deg as shown in Fig. 1(e): for both polarizations the spectra are given by a broad distribution in the mid-infrared region, provided by a combination of single and multiple paramagnons, charge and vibrational excitations, all difficult to disentangle. On the other hand, in a near-grazing-emission geometry (large positive δ values), single spin-flip excitations are prominent for π and suppressed for σ polarization. This is evident at $\delta = +50$ deg for the peak at ~ 350 meV in Fig. 1(e). This incident polarization dependence has been further confirmed by a recent RIXS experiment obtained by using a soft x-ray polarimeter capable of measuring the polarization of the scattered radiation³² simultaneously with the spectral distribution. Therefore we consider the peak at ~ 350 meV at $Q_{\parallel} = 0.4$ rlu ($\delta = +50$ deg) to be a single spin-flip excitation.

In Fig. 2 we show the evolution of the spin-flip spectral component along the $(0,0)$ - $(0.5,0)$ symmetry direction. It appears from the raw data that the paramagnon mode disperses to high energy loss similarly to

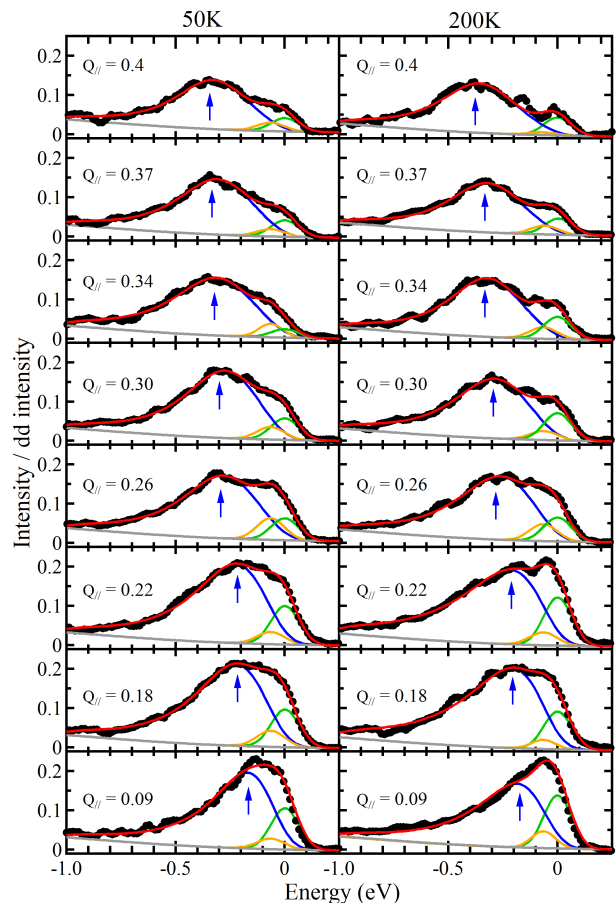


FIG. 2. (color online) The RIXS spectra of OP-Bi2201 along $(0,0)$ - $(0.5,0)$ symmetry direction (black solid circles) at 50 K (left) and 200 K (right). The spectra are decomposed into the dispersive magnetic excitations (blue line), the elastic scattering (green line), the phonon scattering (orange line), and the charge- and dd -excitations background (gray line). The blue arrow indicates the paramagnon peak. The data were collected at grazing-emission using π incident polarization.

that of other superconducting cuprates.⁴⁻⁷ We decompose the spectra into four different contributions:^{5,6} a resolution-limited Gaussian for the elastic peak, an antisymmetrized Lorentzian for the magnetic scattering, a smooth background for the particle-hole continuum and the tail of dd excitations, and a resolution-limited Gaussian for the dominant phonon which is a bond stretching longitudinal optical (LO) mode of ~ 65 meV previously observed by Raman³³ and high-resolution inelastic x-ray scattering.³⁴ Its strong coupling to electrons, manifested in ARPES by a kink in the electronic state dispersion,^{34,35} constitutes a significant part in RIXS. Within the present experimental accuracy we can not determine the phonon dispersion, and the crucial implications of its observation in Cu L_3 RIXS will be discussed elsewhere.³⁶

We track the paramagnon peak as denoted by the

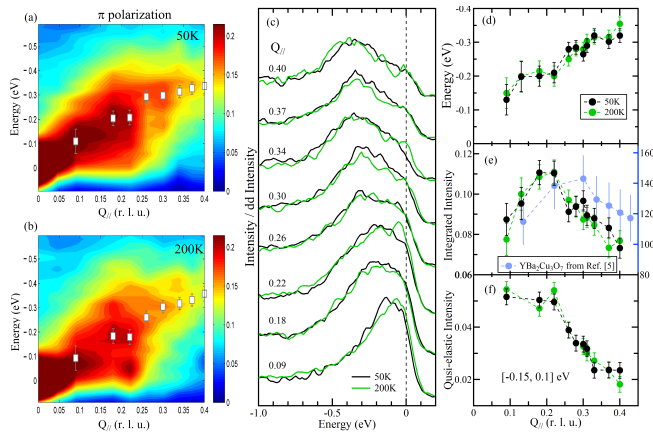


FIG. 3. (color online) Energy/momentum intensity false-color maps of RIXS spectra along $(0,0)-(0.5,0)$ symmetry direction measured at (a) 50 K and (b) 200 K with π polarization on OP-Bi2201. The white solid squares indicate the paramagnon peak positions as determined with the fitting procedure illustrated in Fig. 2. (c) RIXS spectra at 50 K (black) and 200 K (green) at selected Q_{\parallel} . (d) Experimental paramagnon dispersion and (e) the integrated intensity of paramagnon peak at 50K (black) and 200K (green) determined from the fitting procedure. Integrated inelastic intensity of optimally doped $\text{YBa}_2\text{Cu}_3\text{O}_7$ from Ref. 5 is superimposed for comparison (blue). (f) Intensity at $[-0.15, 0.1]$ eV energy window for quasi-elastic signal at 50 K (black) and 200 K (green). Self-absorption correction has been applied to (e) and (f). The error bars represent the uncertainty in the fitting.

blue arrows in Fig. 2, and superimpose it on the energy/momentum intensity map in Fig. 3 for (a) 50 K (below T^*) and (b) 200 K (above T^*). From the maps we note that the intensity of the high energy magnetic excitation shows a decrease above $Q_{\parallel} \simeq 0.22$ rlu for both temperatures; meanwhile one feature appears below 100 meV at $Q_{\parallel} \simeq 0.22$ rlu, which will be discussed subsequently. To visualize if there is any temperature dependence, we overlap the raw spectra measured at the two temperatures in Fig. 3(c). The two sets of spectra are almost identical within the experimental uncertainty, confirming therefore that the effective super-exchange interaction J_{eff} is very weakly temperature dependent.³⁷

The energy and integrated intensity of paramagnon determined from the fitting procedure are compared respectively in Fig. 3(d) and (e) for the two temperatures. In the antiferromagnetic systems the paramagnon intensity is expected theoretically to decrease to zero when approaching the Γ point.^{1,2} From Fig. 3(e) we observe a similar behavior below 0.2 rlu also in OP-Bi2201, although the paramagnon intensity could not be tracked below 0.1 rlu due to the onset, towards Γ , of the elastic peak that hinders any possible sub-100 meV inelastic feature with the present resolution. More interestingly though, the intensity of paramagnon also shows an abrupt drop above $Q_{\parallel} \simeq 0.22$ rlu. In Fig. 3(f) we integrated over $[-0.15, 0.1]$ eV energy window to evaluate

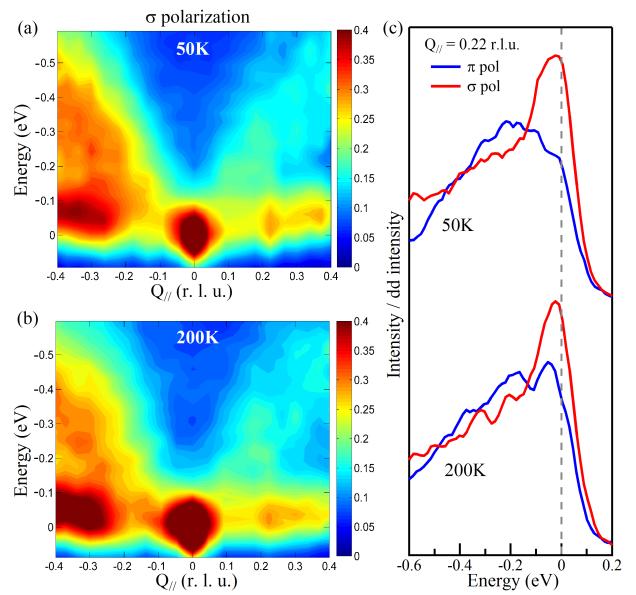


FIG. 4. (color online) Energy/momentum intensity false-color maps of RIXS spectra along $(-0.5,0)-(0.5,0)$ symmetry direction measured at (a) 50 K and (b) 200 K with σ polarization on OP-Bi2201. (c) Polarization comparison of RIXS spectra measured at $Q_{\parallel} = 0.22$ rlu at 50 K and 200 K.

the quasi-elastic intensity: the intensity shows a step (or a peak) at $Q_{\parallel} \simeq 0.22$ rlu and then decreases with momentum for both temperatures. We have applied self-absorption correction³⁸ to the intensity and found that the change of intensity is less than 10% near the Brillouin zone boundary, which can not explain the strong depression of intensity above 0.22 rlu here (nearly 40% decrease around the Brillouin zone boundary). For bismuth cuprates the small correction for the spectra normalized to dd intensity is due to the relative large pre-edge signal of x-ray absorption spectra, originated from the large non-resonant absorption of bismuth. The coincident intensity drop of paramagnon and quasi-elastic signal indicates a nontrivial effect. We notice that for optimally doped $\text{YBa}_2\text{Cu}_3\text{O}_7$ in Refs. 5, the integrated inelastic intensity shows a decrease above 0.3 rlu, a wave vector characterizing charge order²⁰ and bond-buckling phonon anomaly.³⁹ Therefore, charge order and phonon anomaly might play a role in our OP-Bi2201 too, as discussed below. We also notice that around $Q_{\parallel} \simeq 0.22$ rlu the paramagnon energy in Fig. 3(d) seems to deviate from a smooth dispersion, which deserves further investigation as well.

IV. DISCUSSION

A. Intensity maps of RIXS spectra

The concurrent intensity drop of paramagnon and quasi-elastic signal around $Q_{\parallel} = 0.22$ rlu are probably not a fortuitous coincidence. In the map of Fig. 3(b), we can directly observe a feature below 100 meV at $Q_{\parallel} \simeq 0.22$ rlu. This can be put in relation with other intriguing phenomena taking place in Bi2201, such as charge order and strong electron-phonon coupling. Charge order, with $Q_{CO} = 0.243$ rlu, has been observed recently in underdoped Bi2201 ($T_c = 30$ K) by resonant x-ray scattering¹⁷ and, with $Q_{\parallel} \sim 0.28$ rlu, in OP-Bi2212 by RIXS.¹⁹ Here the wave-vector of the low energy feature, i.e. 0.22 rlu, is compatible with the one of a charge order signal. However the persistence of the feature up to 200 K, above the presumed charge order temperature, seems in contrast with the commonly observed temperature dependence of the charge order in hole-doped cuprates.^{13,17} In the present RIXS data on OP-Bi2201 we did not find an evidence for charge order, possibly because of the excessive disorder, known to be higher in Bi2201 than in Bi2212.^{18,40} Unfortunately the lack of an unambiguous evidence of charge order in the present sample does not allow us to make a direct connection, on that issue, to the ARPES results, which showed particle-hole symmetry breaking²² and a phase transition below the pseudogap temperature.²³ On the other hand we can exploit the richness of the RIXS spectra.

The assignment of the low energy feature can be inspired by observing the RIXS colormaps of Fig. 4(a) and 4(b), where the σ polarization was used. At positive Q_{\parallel} the σ polarization enhances the non-spin-flip final states, including bi-magnon-like magnetic excitations, particle-hole pair generation and phonons; at negative Q_{\parallel} the spin-flip and non-spin-flip excitations have similar intensity. We can unambiguously observe a peak below 100 meV at $Q_{\parallel} = +0.22$ rlu: this peak is stronger with σ than π polarization, as highlighted by the spectra comparison in Fig. 4(c), a clear demonstration of its non-spin-flip character. Its energy is fully compatible with a phonon excitation. This assignment is confirmed by the data at negative Q_{\parallel} , where the phonon peak has an almost flat dispersion but a clear increase in intensity beyond -0.25 rlu. Interestingly, inelastic x-ray scattering measurement on optimally doped $\text{Bi}_2\text{Sr}_{1.6}\text{La}_{0.4}\text{CuO}_{6+\delta}$ found that the Cu-O bond stretching (BS) phonon shows a softening and an anomalously broad line-shape around 0.22-0.25 rlu.³⁴ The crossing of two longitudinal phonon modes and/or the anomalous broadening of the BS phonon may have a relation to the strong phonon signal around 0.22 rlu in RIXS. Moreover phonon softening and broadening has been observed around the charge ordering wave-vector in several copper oxide superconductors,^{39,41,42} revealing the correlation between charge order and phonon anomalies in experiments other than RIXS. What RIXS is adding here

in the specific case of OP-Bi2201, is the coincidence of phonon and paramagnon intensity anomalies, appearing in the putative charge-order wave-vector region. Interestingly enough, optimally doped YBCO shows a similar maximum of the paramagnon intensity around its own charge-order wave-vector (0.30 rlu), as shown in figure 3(e). The q -dependence of the phonon intensity in RIXS and its relation with charge order goes beyond the scope of this article and will be treated more systematically elsewhere.³⁶ Moreover in the near future better resolved and more systematic RIXS measurements will help to clarify the connection of charge-order and phonon anomaly with the paramagnon energy and intensity evolution.

B. Relation between J_{eff} and T_c

In Fig. 5 we compare the RIXS spectra of OP-Bi2201 and OP-Bi2212 at large Q_{\parallel} for π polarization. In panel (a), the two data sets for OP-Bi2201 (one at 50 K with 150 meV resolution, one at 40 K with 300 meV resolution) are compatible with each other, once the difference in resolution is taken into account. For OP-Bi2212 (40 K, 300 meV resolution) we observe that the dd multiplet is more extended towards higher energy, due to the $d_{3z^2-r^2}$ final state being more separated from the $d_{x^2-y^2}$,

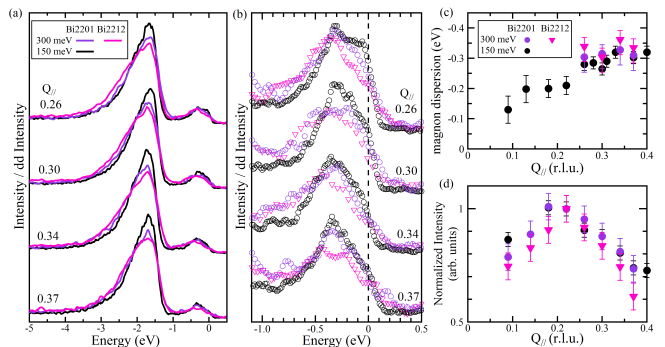


FIG. 5. (color online) (a) Comparison of RIXS spectra of OP-Bi2201 and OP-Bi2212 at large Q_{\parallel} measured with π polarization. Two data sets were collected for OP-Bi2201, at 50 K and 40 K with energy resolution of 150 meV (black) and 300 meV (purple) respectively; OP-Bi2212 data were collected at 40 K with energy resolution of 300 meV (magenta). (b) Enlarged view of the low energy portion. (c) The paramagnon energies of OP-Bi2201 and OP-Bi2212 from the fitting of the spectra with experimental resolution of 300 meV are overlaid with paramagnon energy of OP-Bi2201 at 50 K reproduced from Fig. 3(d). The large error bars are due to the fitting uncertainty for the lower resolution spectra. (d) Integrated intensities of RIXS spectra with energy window $[-0.8, 0]$ eV, normalized to the respective value at $Q_{\parallel} = 0.22$ rlu. Self-absorption correction has been applied to the intensities. The error bars represent the uncertainty in determining the spectral weight.

due to the absence of one apical oxygen in the bilayer compound with respect to the single layer Bi2201. Panel (b) shows an enlarged view of the low energy portion. The paramagnon energies are similar in the two samples. Following the usual fitting procedure,^{5,6} we obtain that the paramagnon energy at zone boundary is ~ 350 meV, as shown in Fig. 5(c). At small Q_{\parallel} the fitting for spectra with lower resolution is too uncertain and we cannot plot the corresponding points in panel (c). We present the integrated intensities for OP-Bi2201 and OP-Bi2212 in Fig. 5(d), which are very similar with a consistent drop above ~ 0.22 rlu, suggesting a common interplay in Bi-based cuprate family.

These results are in stark contrast with those recently published by Dean et al.,⁴³ who have found that the paramagnon energy at zone boundary is substantially higher in $\text{Bi}_2\text{Sr}_2\text{Ca}_2\text{Cu}_3\text{O}_{10+\delta}$ (Bi-2223, $T_c = 109$ K) than in $\text{Bi}_{2+x}\text{Sr}_{2-x}\text{CuO}_{6+\delta}$ (Bi-2201, $T_c \simeq 1$ K). In Ref. 43 the paramagnon energies are assigned at 295 meV for Bi-2201 and 347 meV for Bi-2223 close to $(1/2, 0, L)$. From this result the authors argued that T_c scales monotonically with J_{eff} . However, previous results in Bi2212 had rather shown an opposite trend, i.e., the softening with doping of the magnetic excitation energy, namely from ~ 350 meV in the heavily underdoped nonsuperconducting sample to ~ 300 meV in the optimally doped one ($T_c = 92$ K).⁷ Here we find that the paramagnon energies of OP-Bi2201 ($T_c \simeq 34$ K) and OP-Bi2212 ($T_c \simeq 96$ K) are indeed similar to that of Bi-2223 ($T_c = 109$ K) and of heavily underdoped Bi2212. Therefore our results confirm for the Bi22nm family what was already known for YBCO and LSCO,^{5,6,8} that the value of the magnetic excitation energy at zone boundary does not correlate directly to T_c . The exception found in Ref. 43 is possibly due to the different local structure (Cu-O distance, Cu-O-Cu bond angle) of the Bi-doped compound, chosen for its especially low T_c at optimal doping. Although there is a good probability that magnetic fluctuations play a decisive role in high- T_c superconductivity, the maximum of

T_c for different materials may be more strongly influenced by other factors than just the value of the superexchange coupling.

V. CONCLUSIONS

In the RIXS spectra measured with the appropriate conditions (π polarization, positive Q_{\parallel} values), we have observed the simultaneous intensity decrease of the paramagnon and the quasi-elastic signal above ~ 0.22 rlu, the wave-vector of the putative charge-order in OP-Bi2201. The tiny temperature dependence and the evidence of a concurrent onset, with σ polarization, of the phonon signal at that special wave-vector, hint at a combined effect, on the magnetic excitation spectrum, of electron-phonon coupling and incipient charge-order. Further insight into this issue could come from considering the influence of phonon and charge order on the spin dynamical structure factor. Moreover we give here a further confirmation of the robustness of magnetic excitations across the phase diagram of high T_c cuprate superconductors. There is, however, an increasing general evidence that, in cuprates, spin excitations get coupled, via the electron-phonon interaction, to both lattice modes and charge order, therefore providing a ubiquitous ingredient for the superconductivity pairing mechanisms. A better clarification of this three-actors scenario (spin excitations, electron-phonon coupling, charge order) will require further systematic use of high resolution resonant elastic and inelastic x-ray scattering.

ACKNOWLEDGMENTS

The spectra at the ADDRESS beam line of the Paul Scherrer Institut were measured using the SAXES instrument developed jointly by Politecnico di Milano, SLS, and EPFL. This work is supported by the PIK project POLARIX of the Italian Ministry of Research (MIUR).

* yingying.peng@polimi.it

† Present address: European Synchrotron Radiation Facility (ESRF), BP 220, F-38043 Grenoble Cedex, France

‡ Present address: Max-Planck-Institut für Festkörperforschung, Heisenbergstraße 1, D-70569 Stuttgart, Germany

§ Present address: Diamond Light Source, Harwell Science and Innovation Campus, Didcot, Oxon, OX11 0DE, United Kingdom

¹ L. J. P. Ament, G. Ghiringhelli, M. M. Sala, L. Braicovich, and J. van den Brink, Phys. Rev. Lett. 103, 117003 (2009).

² M. W. Haverkort, Phys. Rev. Lett. 105, 167404 (2010).

³ K. Ishii, M. Fujita, T. Sasaki, M. Minola, G. Dellea, C. Mazzoli, K. Kummer, G. Ghiringhelli, L. Braicovich, T. Tohyama, K. Tsutsumi, K. Sato, R. Kajimoto, K. Ikeuchi,

K. Yamada, M. Yoshida, M. Kurooka and J. Mizuki, Nat. Commun. 5, 3714 (2014).

⁴ L. Braicovich, J. van den Brink, V. Bisogni, M. M. Sala, L. J. P. Ament, N. B. Brookes, G. M. De Luca, M. Salluzzo, T. Schmitt, V. N. Strocov, and G. Ghiringhelli, Phys. Rev. Lett. 104, 077002 (2010).

⁵ M. Le Tacon, G. Ghiringhelli, J. Chaloupka, M. M. Sala, V. Hinkov, M. W. Haverkort, M. Minola, M. Bakr, K. J. Zhou, S. Blanco-Canosa, C. Monney, Y. T. Song, G. L. Sun, C. T. Lin, G. M. De Luca, M. Salluzzo, G. Khaliullin, T. Schmitt, L. Braicovich, and B. Keimer, Nat. Phys. 7, 725 (2011).

⁶ M. P. M. Dean, G. Dellea, R. S. Springell, F. Yakhov-Harris, K. Kummer, N. B. Brookes, X. Liu, Y.-J. Sun, J. Strle, T. Schmitt, L. Braicovich, G. Ghiringhelli, I. Bozovic

- and J. P. Hill, *Nat. Mater.* 12, 1019 (2013).
- 7 M. P. M. Dean, A. J. A. James, R. S. Springell, X. Liu, C. Monney, K. J. Zhou, R. M. Konik, J. S. Wen, Z. J. Xu, G. D. Gu, V. N. Strocov, T. Schmitt, and J. P. Hill, *Phys. Rev. Lett.* 110, 147001 (2013).
 - 8 M. Le Tacon, M. Minola, D. C. Peets, M. Moretti Sala, S. Blanco-Canosa, V. Hinkov, R. Liang, D. A. Bonn, W. N. Hardy, C. T. Lin, T. Schmitt, L. Braicovich, G. Ghiringhelli, and B. Keimer, *Phys. Rev. B* 88, 020501 (2013).
 - 9 J. M. Tranquada, B. J. Sternlieb, J. D. Axe, Y. Nakamura and S. Uchida, *Nature (London)* 375, 561 (1995).
 - 10 M. Fujita, H. Goka, K. Yamada, and M. Matsuda, *Phys. Rev. Lett.* 88, 167008 (2002).
 - 11 P. Abbamonte, A. Rusydi, S. Smadici, G. D. Gu, G. A. Sawatzky, and D. L. Feng, *Nat. Phys.* 1, 155 (2005).
 - 12 T. Wu, H. Mayaffre, S. Krämer, M. Horvatic, C. Berthier, W. N. Hardy, R. X. Liang, D. A. Bonn, and M.-H. Julien, *Nature (London)* 477, 191 (2011)
 - 13 G. Ghiringhelli, M. Le Tacon, M. Minola, S. Blanco-Canosa, C. Mazzoli, N. B. Brookes, G. M. De Luca, A. Frano, D. G. Hawthorn, F. He, T. Loew, M. M. Sala, D. C. Peets, M. Salluzzo, E. Schierle, R. Sutarto, G. A. Sawatzky, E. Weschke, B. Keimer, and L. Braicovich, *Science* 337, 821 (2012).
 - 14 A. J. Achkar, R. Sutarto, X. Mao, F. He, A. Frano, S. Blanco-Canosa, M. Le Tacon, G. Ghiringhelli, L. Braicovich, M. Minola, M. Moretti Sala, C. Mazzoli, R. Liang, D. A. Bonn, W. N. Hardy, B. Keimer, G. A. Sawatzky, and D. G. Hawthorn, *Phys. Rev. Lett.* 109, 167001 (2012).
 - 15 J. Chang, E. Blackburn, A. T. Holmes, N. B. Christensen, J. Larsen, J. Mesot, R. Liang, D. A. Bonn, W. N. Hardy, A. Watenphul, M. v. Zimmermann, E. M. Forgan, and S. M. Hayden, *Nat. Phys.* 8, 871 (2012).
 - 16 E. Blackburn, J. Chang, M. Hucker, A. T. Holmes, N. B. Christensen, R. Liang, D. A. Bonn, W. N. Hardy, U. Rutt, O. Gutowski, M. v. Zimmermann, E. M. Forgan, and S. M. Hayden, *Phys. Rev. Lett.* 110, 137004 (2013).
 - 17 R. Comin, A. Frano, M. M. Yee, Y. Yoshida, H. Eisaki, E. Schierle, E. Weschke, R. Sutarto, F. He, A. Soumyanarayanan, Y. He, M. Le Tacon, I. Elfimov, J. E. Hoffman, G. Sawatzky, B. Keimer, and A. Damascelli, *Science* 343, 390 (2014).
 - 18 E. H. da Silva Neto, P. Aynajian, A. Frano, R. Comin, E. Schierle, E. Weschke, A. Gyenis, J. S. Wen, J. Schneeloch, Z. J. Xu, S. Ono, G. D. Gu, M. Le Tacon, and Ali Yazdani, *Science* 343, 393 (2014).
 - 19 M. Hashimoto, G. Ghiringhelli, W.-S. Lee, G. Dellea, A. Amorese, C. Mazzoli, K. Kummer, N. B. Brookes, B. Moritz, Y. Yoshida, H. Eisaki, Z. Hussain, T. P. Devereaux, Z.-X. Shen, and L. Braicovich, *Phys. Rev. B* 89, 220511(R) (2014).
 - 20 S. Blanco-Canosa, A. Frano, E. Schierle, J. Porras, T. Loew, M. Minola, M. Bluschke, E. Weschke, B. Keimer, M. Le Tacon, *Phys. Rev. B* 90, 054513 (2014).
 - 21 E. H. da Silva Neto, R. Comin, F. He, R. Sutarto, Y. Jiang, R. L. Greene, G. A. Sawatzky, and A. Damascelli, *Science* 347, 6219 (2015).
 - 22 M. Hashimoto, R.-H. He, K. Tanaka, J.-P. Testaud, W. Meevasana, R. G. Moore, D. H. Lu, H. Yao, Y. Yoshida, H. Eisaki, T. P. Devereaux, Z. Hussain and Z.-X. Shen, *Nat. Phys.* 6, 414 (2010).
 - 23 R.-H. He, M. Hashimoto, H. Karapetyan, J. D. Koralek, J. P. Hinton, J. P. Testaud, V. Nathan, Y. Yoshida, Hong Yao, K. Tanaka, W. Meevasana, R. G. Moore, D. H. Lu, S.-K. Mo, M. Ishikado, H. Eisaki, Z. Hussain, T. P. Devereaux, S. A. Kivelson, J. Orenstein, A. Kapitulnik, and Z.-X. Shen, *Science* 331, 1579 (2011).
 - 24 G. Ghiringhelli, A. Piazzalunga, C. Dallera, G. Trezzi, L. Braicovich, T. Schmitt, V. N. Strocov, R. Betemps, L. Patthey, X. Wang, and M. Grioni, *Rev. Sci. Instrum.* 77, 113108 (2006).
 - 25 V. N. Strocov, T. Schmitt, U. Flechsig, T. Schmidt, A. Imhof, Q. Chen, J. Raabe, R. Betemps, D. Zimoch, J. Krempasky, X. Wang, M. Grioni, A. Piazzalunga and L. Patthey, *J. Synchrotron Radiat.* 17, 631 (2010).
 - 26 C. Dallera, E. Puppini, G. Trezzi, N. Incorvaia, A. Fasana, L. Braicovich, N. B. Brookes, and J. B. Goedkoop, *J. Synchrotron Radiat.* 3, 231 (1996).
 - 27 L. Braicovich, M. Moretti Sala, L. J. P. Ament, V. Bisogni, M. Minola, G. Balestrino, D. Di Castro, G. M. De Luca, M. Salluzzo, G. Ghiringhelli, and J. van den Brink, *Phys. Rev. B* 81, 174533 (2010).
 - 28 M. Moretti Sala, V. Bisogni, C. Aruta, G. Balestrino, H. Berger, N. B. Brookes, G. M. de Luca, D. Di Castro, M. Grioni, M. Guarise, P. G. Medaglia, F. Miletto Granozio, M. Minola, P. Perna, M. Radovic, M. Salluzzo, T. Schmitt, K. J. Zhou, L. Braicovich and G. Ghiringhelli, *New Journal of Phys.* 13, 043026 (2011).
 - 29 M. Minola, D. Di Castro, L. Braicovich, N. B. Brookes, D. Innocenti, M. Moretti Sala, A. Tebano, G. Balestrino, and G. Ghiringhelli, *Phys. Rev. B* 85, 235138 (2012).
 - 30 L. Hozoi, L. Siurakshina, P. Fulde and J. van den Brink, *Sci. Rep.* 1, 65 (2011).
 - 31 C. J. Jia, E. A. Nowadnick, K. Wohlfeld, Y. F. Kung, C.-C. Chen, S. Johnston, T. Tohyama, B. Moritz, and T. P. Devereaux, *Nat. Commun.* 5, 4314 (2014).
 - 32 L. Braicovich, M. Minola, G. Dellea, M. Le Tacon, M. Moretti Sala, C. Morawe, J.-Ch. Peffen, R. Suprunet, F. Yakhov, G. Ghiringhelli, and N. B. Brookes, *Rev. Sci. Instrum.* 85, 115104 (2014).
 - 33 S. Sugai, H. Suzuki, Y. Takayanagi, T. Hosokawa, and N. Hayamizu, *Phys. Rev. B* 68, 184504 (2003).
 - 34 J. Graf, M. d'Astuto, C. Jozwiak, D. R. Garcia, N. L. Saini, M. Krisch, K. Ikeuchi, A. Q. R. Baron, H. Eisaki, and A. Lanzara, *Phys. Rev. Lett.* 100, 227002 (2008).
 - 35 Y. Y. Peng, J. Q. Meng, L. Zhao, Y. Liu, J. F. He, G. D. Liu, X. L. Dong, S. L. He, J. Zhang, C. T. Chen, Z. Y. Xu and X. J. Zhou, *Chin. Phys. Lett.* 30, 067402 (2013).
 - 36 L. Braicovich, et al. unpublished.
 - 37 R. Coldea, S. M. Hayden, G. Aeppli, T. G. Perring, C. D. Frost, T. E. Mason, S.-W. Cheong, and Z. Fisk et al., *Phys. Rev. Lett.* 86, 5377 (2001).
 - 38 M. Minola, G. Dellea, H. Gretarsson, Y. Y. Peng, Y. Lu, J. Porras, T. Loew, F. Yakhov, N. B. Brookes, Y. B. Huang, J. Pellicciari, T. Schmitt, G. Ghiringhelli, B. Keimer, L. Braicovich and M. Le Tacon, arXiv:1502.02583 (2015).
 - 39 D. Reznik, *Physica C* 481, 75-92 (2012).
 - 40 W. D. Wise, K. Chatterjee, M. C. Boyer, T. Kondo, T. Takeuchi, H. Ikuta, Z. J. Xu, J. S. Wen, G. D. Gu, Y. Wang, and E. W. Hudson, *Nat. Phys.* 5, 213 (2009).
 - 41 M. Le Tacon, A. Bosak, S. M. Souliou, G. Dellea, T. Loew, R. Heid, K.-P. Bohnen, G. Ghiringhelli, M. Krisch and B. Keimer, *Nat. Phys.* 10, 52 (2013).
 - 42 E. Blackburn, J. Chang, A. H. Said, B. M. Leu, Ruixing Liang, D. A. Bonn, W. N. Hardy, E. M. Forgan, and S. M. Hayden, *Phys. Rev. B* 88, 054506 (2013).

⁴³ M. P. M. Dean, A. J. A. James, A. C. Walters, V. Bisogni, I. Jarrige, M. Hucker, E. Giannini, M. Fujita, J. Pellicari,

Y. B. Huang, R. M. Konik, T. Schmitt, and J. P. Hill, Phys. Rev. B 90, 220506 (2014).